Technical Note

Characterizing Strength and Failure of Calcium Silicate Hydrate Aggregates in Cement Paste under Micropillar Compression

Rahnuma Shahrin, S.M.ASCE[1]; and Christopher P. Bobko, Ph.D.[2]

Abstract: A new methodology is proposed for investigating compressive failure behavior of cement paste at the micrometer scale. Micropillar geometries are fabricated by focused ion-beam milling on potential calcium-silicate-hydrate (C-S-H) locations identified through energy dispersive spectroscopy (EDS) spot analysis. Uniaxial compression testing of these pillars is performed using nanoindentation equipment. The compressive strength of C-S-H aggregates (225–606 MPa) measured from microcompression tests is found to be consistent with values from multiscale damage and molecular dynamic models. From posttest images, two primary deformation mechanisms at failure were identified; axial splitting and plastic collapse of the entire sample were observed. **DOI: 10.1061/(ASCE)NM.2153-5477.0000137.**
© 2017 American Society of Civil Engineers.

Downloaded from ascelibrary.org by 18.234.201.198 on 11/08/21. Copyright ASCE. For personal use only; all rights reserved.

Introduction

Concrete, the single most widely used material in the world, is a complex heterogeneous material that exhibits different mechanical properties at separate length scales (Constantinides and Ulm 2007; Bernard et al. 2003). Cement paste is the binder and key ingredient of concrete and a hierarchical material itself, with three different levels spanning the range from a few nanometers to hundreds of micrometers (Constantinides and Ulm 2004). The basic minerals involved, calcium-silicate-hydrates (C-S-H), have complicated nonregular molecular structures (Pellenq et al. 2009) at Level 0 (1–100 nm) known as C-S-H globules (Tennis and Jennings 2000). At Level 1 (100 nm–10 μm), these globules pack together to form a granular composite of C-S-H aggregates and pore space. At Level 2 (10–1,000 μm), the C–S–H aggregate acts as a matrix and binds the inclusions of $Ca(OH)_2$, unhydrated cement clinkers, water, and micrometer-range porosity to form cement paste (Hlobil et al. 2015). The highly disordered material C-S-H has an average formula of $1.8CaO \cdot SiO_2 \cdot 4.0H_2O$ (Taylor 1997). Advances in energy dispersive spectroscopy (EDS) analyses have enabled better understanding of the composition variation of C-S-H by measuring approximate ranges of the calcium-to-silicon ratio (Ca/Si) as 1.2–2.3 (Richardson and Groves 1993). Other constituents of cement paste include $Ca(OH)_2$ and a variety of trace compounds.

As the primary phase of cement paste, C-S-H is responsible for strength and other mechanical properties of cement-based materials. Therefore, a fundamental understanding and quantification of the failure behavior of C-S-H at Level 1 is critical for understanding failure at larger scales. Molecular dynamics modeling provides some insight about the material behavior within the globules (Pellenq et al. 2009; Selvam et al. 2009), but the complex granular microstructure of C-S-H aggregates at Level 1 presents a system far too large for feasible atomistic computations. At the microscale, grid nanoindentation testing has been successfully used to measure elastic moduli, creep, and hardness properties of cement paste under complex multiaxial stress states (Constantinides and Ulm 2004, 2007; Vandamme and Ulm 2009). However, direct measurement of compressive strength is not possible by conventional nanoindentation.

Over the last decade, uniaxial compression of focused ion-beam (FIB)-milled micropillars using nanoindentation equipment has become an effective approach to investigate small-scale strength properties (Uchic et al. 2004; Ye et al. 2010; Volkert and Lilleodden 2006; Shim et al. 2009; Korte and Clegg 2009). Yet, few studies have explored the application of microcompression testing to granular and heterogeneous materials, which have a hierarchical microstructure like cement paste (Zhang et al. 2010; Abousleiman et al. 2016; Yilmaz et al. 2015; An et al. 2015; Dewers et al. 2010; Han et al. 2011; Luczynski et al. 2015). Whereas one study used FIB-milled microbeams to assess the tensile strength of cement (Němeček et al. 2016), uniaxial compression tests have never been performed on FIB-milled cement micropillars for assessing their compressive failure behavior. In this work, a new methodology is proposed to provide a quantitative portrait of the failure behavior of cement paste at Level 1. First, EDS spot analysis is used to identify potential location of C-S-H on a cement-paste sample, and then micropillars are milled at these locations. Nanoindentation equipment is used to perform uniaxial compression testing on the micropillars, and scanning electron microscope (SEM) images of the failed pillars are used to help investigate failure deformation mechanisms.

Materials and Methods

Sample parameters were carefully chosen to be representative of the basic form of cement paste. Regular Type I/II cement with a water/cement (w/c) ratio of 0.42 was selected as test material. This cement paste was cured under sealed conditions to achieve full hydration and development of strength for 3 years. Specimens were

[1]Graduate Research Assistant and Ph.D. Candidate, Dept. of Civil, Construction, and Environmental Engineering, North Carolina State Univ., Campus Box 7908, Raleigh, NC 27695-7908. E-mail: rshahri2@ncsu.edu

[2]Adjunct Associate Professor, Dept. of Civil, Construction, and Environmental Engineering, North Carolina State Univ., Campus Box 7908, Raleigh, NC 27695-7908 (corresponding author). E-mail: chris_bobko@ncsu.edu

Note. This manuscript was submitted on February 20, 2017; approved on August 17, 2017; published online on October 17, 2017. Discussion period open until March 17, 2018; separate discussions must be submitted for individual papers. This technical note is part of the ***Journal of Nanomechanics and Micromechanics***, © ASCE, ISSN 2153-5434.

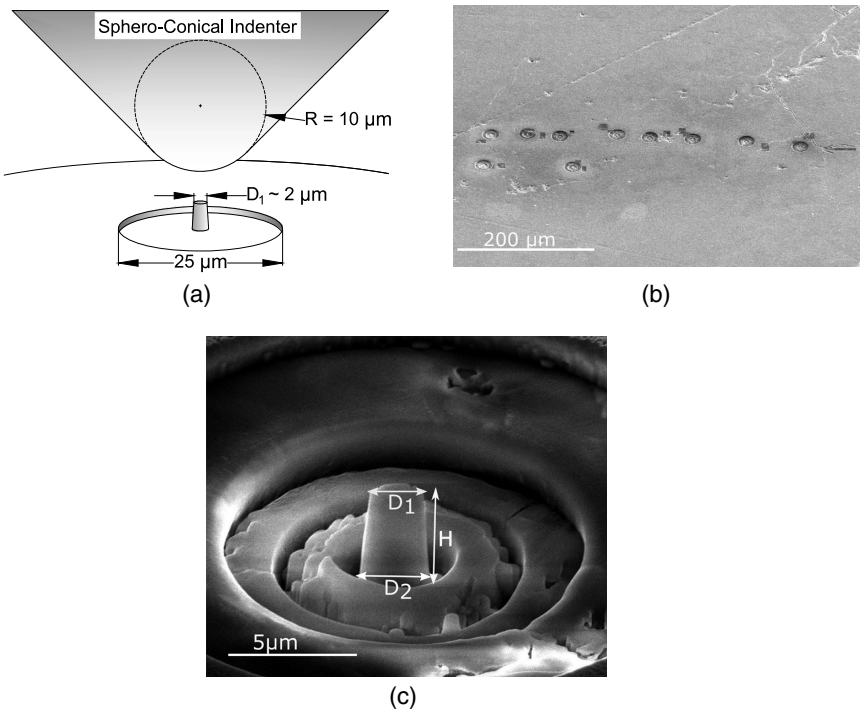

Fig. 1. (a) Schematic of uniaxial compression on the micropillar; (b) SEM image showing position of the micropillars on the cement sample; (c) SEM image of a representative micropillar

cut in a disk shape and again stored in airtight containers to avoid changes in mechanical properties until they were used in the FIB sample preparation process.

Special attention was paid to achieving a flat and smooth surface for subsequent FIB milling. The FIB sample preparation procedure involved cutting very thin slices of cement sample ($15 \times 10 \times 2$ mm) using a Buehler Isomet (Buehler, Lake Bluff, Illinois) low-speed saw. In order to reach appropriate surface roughness, the thin slices were ground for 40 min using a 1,200-grit Silicon Carbaide (SiC) pad (Electron Microscopy Sciences, Hatfield, Pennsylvania) and cleaned with acetone to remove residue. The flat polished sample was then mounted on a SEM stub using double-sided conductive carbon tape. Next, the sample was sputter-coated with a thin layer of gold-palladium (a few nanometers thick).

Because the mechanical properties of C-S-H are the primary focus of this research, pillars were fabricated in areas rich in C-S-H. This was done by acquiring compositional information at different locations of the cement sample through SEM-EDS spot analyses. EDS spectra were collected in a FEI Quanta 3D FEG system (Thermo Fisher Scientific, Hillsboro, Oregon) with an accelerating voltage of 15 kV and beam current of 3.4 nA. The Ca/Si ratio was calibrated using Ca_2SiO_4. Areas primarily composed of calcium, silicon, and oxygen with a Ca/Si ratio of 1.6–2.3 were selected as potential milling locations.

After selecting the area of interest, pillar geometries for microcompression tests were fabricated following the annular milling method (Uchic and Dimiduk 2005; Yang et al. 2009). The operating conditions were optimized to minimize the side-wall taper, milling time, and Ga^+ implantation by investigating a range of beam currents, dwelling times, and current settings. Micropillars were fabricated using the dual-beam FEI Quanta 3D FEG system using a 30-keV focused Ga-ion beam. A series of concentric annular rings with decreasing diameter were milled with beam current gradually decreasing in the 1 nA–100 pA range. This stepwise sequence of removing materials created a 25-μm-diameter trench around the pillar [Fig. 1(a)]. The entire milling process was closely monitored by acquiring secondary electron images at frequent intervals. The trench helps in identification of the pillars with the nanoindentation system's optical microscope. During tests, it also ensures that the indenter tip is in contact with only the pillar top and not surrounding material. Moreover, the trench facilitates measurement of pillar dimensions and inspection of pillar geometry after failure. After FIB milling, the cement samples were stored in airtight SEM sample storage containers.

An overview image shows the relative location and appearance of the micropillars on the cement surface [Fig. 1(b)]. Geometric details of these 10 micropillars are provided in Table 1. Pillars made by annular methods always have a tapering in the side walls, which is quantified by the taper angle, α. High-magnification SEM images of individual pillars were collected during milling, which provide the top diameter, D_1, and bottom diameter, D_2, and height, H, of micropillars [Fig. 1(c)]. The aspect ratio $\{H/[(D_1 + D_2)/2]\}$ of these pillars varies in the range of 1.4–2.

Uniaxial compression was applied to each pillar using a CSM Instruments (Anton Paar USA, Ashland, Virginia) ultranano hardness tester (UNHT) with a 20-μm-diameter spheroconical tip [Fig. 1(a)]. Because of the relatively large diameter of tip in relation to the pillar, the contact area of the tip is very blunt. Practically, the spherical tip acts as a flat punch, with the advantage that when the tip is concentrically aligned with the micropillar, contact between two parallel surfaces is automatically satisfied and only normal force is transmitted to the pillar. To ensure positioning accuracy, the indenter–optical microscope distance was calibrated prior to each test.

Load-controlled single-cycle microcompression tests were performed under a constant loading rate of 0.8 mN/min up to failure. Failure of the pillars was marked by sudden drop of load and displacement jumps. The unloading process was manually initiated for each test as soon as the pillar failed, instead of compressing to a prescribed maximum load. This avoided overcompression of the

Downloaded from ascelibrary.org by 18.234.201.198 on 11/08/21. Copyright ASCE. For personal use only; all rights reserved.

Table 1. Dimension and Mechanical Properties of the Tested Micropillars

Pillar number	D_1 (μm)	D_2 (μm)	H (μm)	Aspect ratio	Taper angle α (degrees)	f_c (MPa)	E (GPa)
P-1	2.48	2.86	3.88	1.5	2.8	323	6.0
P-2	2.48	2.73	3.84	1.5	1.9	246	9.3
P-3	2.55	2.56	4.5	1.8	0.1	225	6.3
P-4	2.39	2.82	4.72	1.8	2.6	606	12.7
P-5	2.01	2.79	3.445	1.4	6.5	585	7.1
P-6	2.18	2.8	4.455	1.8	4.0	490	8.9
P-7	1.93	2.75	4.775	2.0	4.9	334	10.5
P-8	2.17	2.73	4.2	1.7	3.8	540	8.3
P-9	2.18	2.83	4.315	1.7	4.3	515	7.7
P-10	2.23	2.7	4.665	1.9	2.9	404	5.0

pillar, which allowed subsequent SEM imaging to capture the deformed shapes at or right after failure. Calculation of compressive strength was done using the maximum attained force before failure, F_Y, and the minimum (top) cross-sectional area of the pillar where failure was most likely to initiate because of higher stress (Han et al. 2011; Yilmaz et al. 2013; Bharathula et al. 2010; Frick et al. 2008). The compressive strength, f_c was estimated

$$f_c = \frac{4F_Y}{\pi D_1^2} \tag{1}$$

Evaluation of the stress-strain values from load-displacement data was done using the formula proposed by Han et al. (2011), which accounts for the compliance of the underlying material by applying Sneddon's (1965) formula. Normalized stress, σ_n, and strain, ε_n, of slightly tapered and fixed-ended pillars were calculated

$$\varepsilon_n = \frac{\delta}{H} \tag{2}$$

$$\sigma_n = \left(\frac{4}{\pi D_1 D_2} + \frac{1-\nu^2}{D_2 H}\right) F \tag{3}$$

where δ = displacement of the pillar upon applied load of F; and $\nu = 0.24$ = Poisson's ratio of C-S-H (Constantinides and Ulm 2004). Elastic modulus, E, is calculated from the elastic portion of the stress-strain diagram (loading part) through least-squares linear regression

$$E = \frac{d\sigma_n}{d\varepsilon_n} \tag{4}$$

Results and Discussion

The load-displacement behavior of the tested pillars was reproducible with similar trends (Fig. 2). Each curve consisted of three individual stages, namely an initial linear-elastic response followed by a relatively short nonlinear response and then failure upon reaching a critical load. The loading time was relatively short, and the pastes were more than 3 years old so creep strains are considered to be negligible.

Failure of a pillar is marked by sudden plateau or drop in load followed by large displacement bursts (pop-in) events. From careful examination of all the load-displacement curves, two different mechanical response patterns were identified [Figs. 2(a and b)]. The first group of pillars collapsed at comparatively low load with a sudden significant drop in the load where only few data points were acquired in the failure zone [Fig. 2(a)]. Conversely, for the second group of pillars, a small load drop followed by a jagged plateau and large displacement bursts (pop-ins) were visible in the failure zone [Fig. 2(b)]. These kinds of horizontal pop-ins were reported in cases of wood, ceramic, and dental-enamel micropillars (Zhang et al. 2010; Korte and Clegg 2009; Yilmaz et al. 2015). Furthermore, these second group of pillars failed at relatively high loads and consequently exhibited higher strength than the previous group of pillars.

Postcompression images from a variable-pressure scanning electron microscope at 45° tilt were used for characterizing the failure behavior. From the posttest images, it was clear that the failure mechanisms can be broadly classified as splitting versus crushing failure of the micropillar. These observations were consistent with the two distinct mechanical response patterns discussed earlier. Images of the first group revealed that the main body of these pillars were found standing with portions showing signs of axial splitting. Failure occurred by formation of vertical cracks. In most cases, a single vertical crack was found to pass close to the pillar center [Fig. 2(c)]. In a few cases, cracks and splitting were found on the side walls, whereas the central portion of the pillar remained mostly intact [Fig. 2(d)]. Failure by vertical cracking is often reported in compressive strength testing of macroscopic concrete cylinders (ASTM 2001).

The second group of pillars, in contrast, failed by complete collapse of the sample. Failure occurred by plastic crushing of either the entire pillar [Fig. 2(e)] or the top part of the pillar [Fig. 2(f)]. Similar fracture patterns were observed for uniaxial compression of dental-enamel micropillars (Yilmaz et al. 2013, 2015). The visual evaluation of failure mode, however, is somewhat limited. First, recalling that unloading of the pillars was initiated manually after failure, there remains a possibility of some pillars being more compressed than others. Second, images could only be obtained after unloading so any possible intermediate failure mechanisms could not be observed. Despite these limitations, the different failure patterns seem to be closely associated with the different characteristic shapes of the load-displacement curve.

The compressive strength [Eq. (1)] of C-S-H micropillars from the 10 micropillar tests including failure by both axial splitting and plastic crushing varied in the range of 225–606 MPa (Table 1). Such variability is expected because C-S-H is a highly complex material that shows significant compositional variation with a granular aggregate morphology. Moreover, previous investigations on cement paste using standard nanoindentation methods have suggested the presence of distinct low-density (LD) and high-density (HD) C-S-H packings with different elastic modulus (Constantinides and Ulm 2007). Therefore, variations observed in compressive strength results might be also associated with the presence of these distinct C-S-H packings.

The strength properties of cement paste at the Level-1 scale has not yet been well investigated. The limited available literature that has investigated strength of C-S-H at different length scales and using different frameworks is summarized here in the context of the new experimental results. At the Level 0 scale, molecular dynamics

Downloaded from ascelibrary.org by 18.234.201.198 on 11/08/21. Copyright ASCE. For personal use only; all rights reserved.

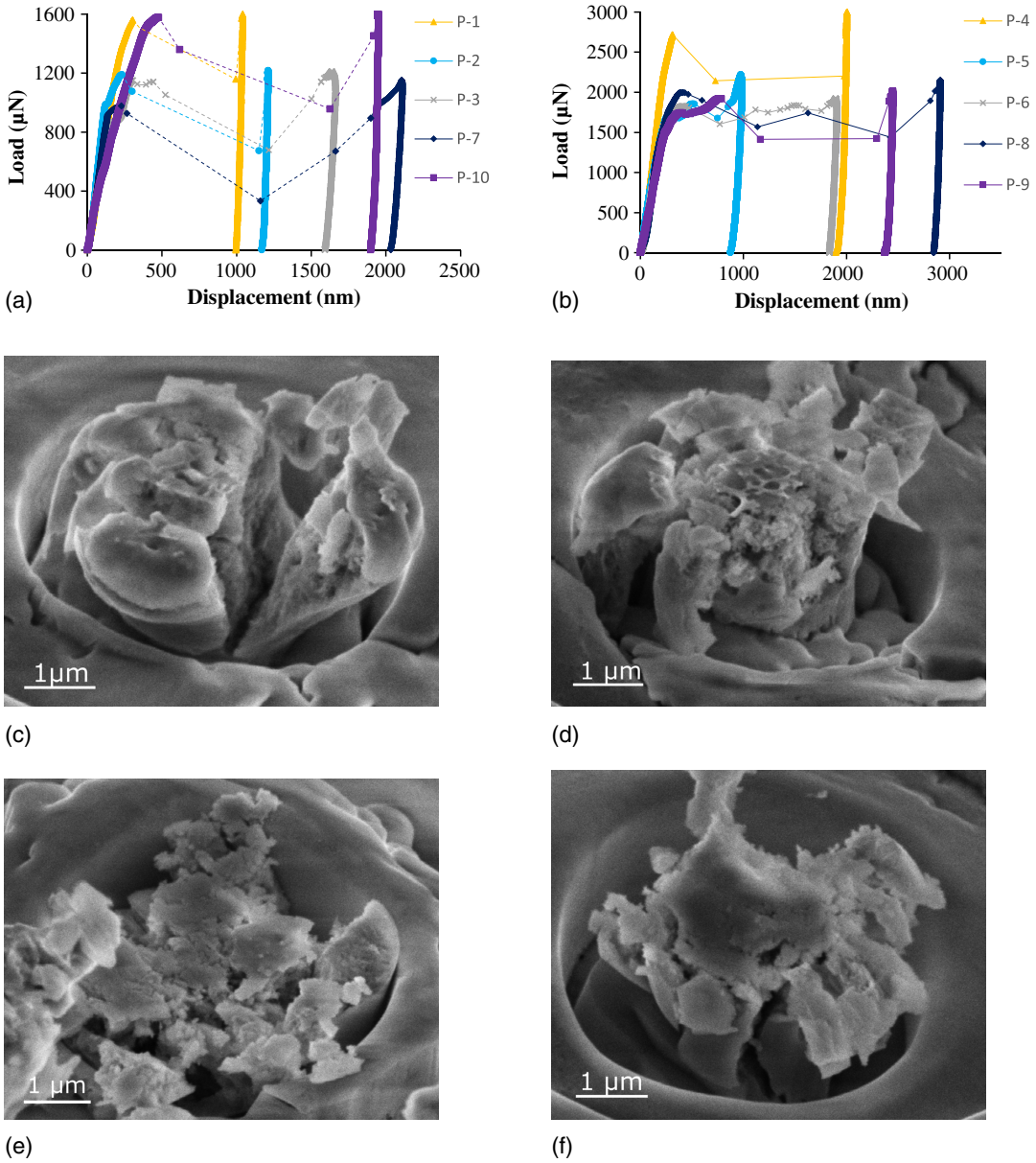

Fig. 2. Load-displacement behaviour of pillars collapsed by (a) cracking; (b) crushing; (c) posttest images showing axial; (d) side-wall cracks; (e) posttest images showing crushing of entire pillar; (f) top part of pillar

simulations predicted the shear strength of individual globules to vary in the range of 1–3 GPa for wet and dry conditions (Pellenq et al. 2009). Molecular dynamics simulation of uniaxial tension and compression performed on a C-S-H atomic structure (1–5 nm) provided ultimate tensile strength and compressive strength values of 3.5 and 15 GPa, respectively (Selvam et al. 2009). That study, however, did not consider the presence of porosity in C-S-H, which would be expected to reduce these values.

Němeček et al. (2016) used microbeam bending tests to estimate tensile strength of C-S-H intermixed with other hydration products in the range of 264–700 MPa. These beams, however, are relatively large (20-μm length) compared with the length scales of individual C-S-H phases and may reflect the response of a heterogonous composite. In addition, use of relatively a high beam current in the final milling step [1 nA in Němeček et al. (2016) compared with 0.1 nA in this study] might have led to a large amount of Ga^+ implantation in the porous microstructure and an increase in measured tensile strength.

In the framework of continuum micromechanics, Pichler and Hellmich (2011) and Pichler et al. (2013a) calculated deviatoric strength of microscopic hydrates to be 69.9 MPa based on an elasto-brittle multiscale model for cementitious materials. Using Mohr-Coulomb parameters from finite-element reanalysis of nanoindentation results, the corresponding model predicted uniaxial compressive strength of low-density C-S-H of 123.5 MPa, which is slightly lower than, but in the same order of magnitude as, the experimental results presented here (Pichler et al. 2013b; Sarris and Constantinides 2013). Furthermore, in modeling hydrate foam in the first step of homogenization, Pichler et al. (2013a) used a representative volume element (RVE) of 20 μm, which is considerably larger than the average diameter of the tested micropillars in the present study. Moreover, the input parameters used for homogenization, bulk, and shear modulus of "hydration products," are not properties specific to LD C-S-H, but rather calculated as an average over all type of hydrates, including ettringite, portlandite, and C-S-H of different mass densities from an almost-pure-hydrate

Downloaded from ascelibrary.org by 18.234.201.198 on 11/08/21. Copyright ASCE. For personal use only; all rights reserved.

cement paste. These two factors might have caused the differences in strength prediction.

Hlobil et al. (2016, 2015) performed multiscale damage modeling and inverse analysis to estimate compressive strength of cement paste at different length scales. They reported compressive strength of 2.5 GPa for C-S-H globules at Level 0 and 528 MPa for LD C-S-H at Level 1. This is in very good agreement with the present study's results, particularly with the pillars showing plastic crushing with an average compressive strength of 547 MPa. However, the finite-element simulations did not consider the possibility of having weaker links in the microstructure. Therefore, it is possible that the micropillars failing through plastic crushing in the present study are located on volumes that do not contain any preexisting weak interface or link in the microstructure. Micropillars showing axial splitting, on the other hand, may have some weak link or interface in the microstructure that is contributing to early crack nucleation and reduction of strength. However, more test results are needed to better understand the two failure modes.

In general, significant reduction in strength is expected to be observed with each increasing hierarchy level because of the presence of porosity and other inclusions. The compressive strength of macroscopic cement paste lies in the range of 20–60 MPa. Thus compressive strength for C-S-H aggregate at Level 1 measured in the current study seems to be in reasonable agreement with the upper and lower limiting values from analysis and measurements at smaller and larger scales.

Initial elastic modulus values were calculated from the slope of the stress-strain curves [Eq. (4)] and are tabulated in Table 1. These observed values for elastic modulus are lower than literature reported results for LD and HD C-S-H based on conventional nanoindentation (Constantinides and Ulm 2004). Many researchers have reported substantially smaller modulus values in microcompression compared with standard nanoindentation (Yilmaz et al. 2013; Yang et al. 2009; Uchic et al. 2003; An et al. 2015). One possible explanation for this mismatch is the fundamental difference between the two approaches (An et al. 2015). Nanoindentation produces a complex triaxial stress state in the vicinity of the indenter, whereas microcompression results in a uniaxial stress state. Moreover, in nanoindentation (Oliver and Pharr 2004) and also some microcompression studies (Yilmaz et al. 2015; Frick et al. 2008), elastic modulus is calculated from unloading slope, which is considered to be fully elastic. However, in this study, the pillars were loaded until brittle failure; hence, unloading slopes could not be used for estimating elastic modulus values. Additionally, initial nonperfect contact between the pillar and indenter might result in misalignment in the system, which leads to underestimation of the elastic modulus (Uchic and Dimiduk 2005; Zhang et al. 2006). Finally, some material-specific experimental factors could play a role. Cement is a porous material containing entrapped air and water; hence the very high vacuum pumping in FIB might damage the material, resulting in additional loss of stiffness. FIB-induced damage caused by Ga^+ ion implantation could also affect the mechanical properties.

Conclusions

In summary, this study has developed a new methodology to investigate compressive failure behavior of cement paste at the micrometer scale. The method involves EDS spot analysis for identifying potential C-S-H locations, fabrication of micropillars using FIB milling, and uniaxial compression testing of these pillars using nanoindentation equipment. From posttest images, two primary deformation mechanisms at failure were identified; axial splitting and plastic collapse of the entire sample were observed. The compressive strength of C-S-H aggregates (225–606 MPa) measured from microcompression tests was consistent with values from multiscale damage and molecular-dynamic models.

Acknowledgments

This work was supported by the National Science Foundation (Award No. 1433054) and North Carolina State University (NCSU). FIB milling and SEM imaging was performed at the Analytical Instrumentation Facility (AIF) at NCSU, which is supported by the State of North Carolina and the National Science Foundation (Award No. ECCS-1542015). The authors would like to specially thank Roberto Garcia from AIF for his technical support with the FIB system.

References

Abousleiman, Y., et al. (2016). "The granular and polymer composite nature of kerogen-rich shale." *Acta Geotechnica*, 11(3), 573–594.

An, B., Wang, R., Arola, D., and Zhang, D. (2015). "Damage mechanisms in uniaxial compression of single enamel rods." *J. Mech. Behav. Biomed. Mater.*, 42, 1–9.

ASTM. (2001). "Standard test method for compressive strength of cylindrical concrete specimens." *ASTM C39–86*, West Conshohocken, PA.

Bernard, O., Ulm, F., and Lemarchand, E. (2003). "A multiscale micromechanics-hydration model for the early-age elastic properties of cement-based materials." *Cem. Concr. Res.*, 33(9), 1293–1309.

Bharathula, A., Lee, S., Wright, W. J., and Flores, K. M. (2010). "Compression testing of metallic glass at small length scales: Effects on deformation mode and stability." *Acta Materialia*, 58(17), 5789–5796.

Constantinides, G., and Ulm, F. (2004). "The effect of two types of CSH on the elasticity of cement-based materials: Results from nanoindentation and micromechanical modeling." *Cem. Concr. Res.*, 34(1), 67–80.

Constantinides, G., and Ulm, F. (2007). "The nanogranular nature of C–S–H." *J. Mech. Phys. Solids*, 55(1), 64–90.

Dewers, T., Boyce, B., Buchheit, T., Heath, J., Chidsey, T., and Michael, J. (2010). "Micropillar compression technique applied to micron-scale mudstone elasto-plastic deformation." *American Geophysical Union Fall Meeting Abstracts*, American Geophysical Union, Washington, DC, 1882.

Frick, C., Clark, B., Orso, S., Schneider, A., and Arzt, E. (2008). "Size effect on strength and strain hardening of small-scale [111] nickel compression pillars." *Mater. Sci. Eng. A*, 489(1), 319–329.

Han, L., Wang, L., Song, J., Boyce, M. C., and Ortiz, C. (2011). "Direct quantification of the mechanical anisotropy and fracture of an individual exoskeleton layer via uniaxial compression of micropillars." *Nano Lett.*, 11(9), 3868–3874.

Hlobil, M., Šmilauer, V., and Chanvillard, G. (2015). "Multiscale micromechanical damage model for compressive strength based on cement paste microstructure." *10th Int. Conf. on Mechanics and Physics of Creep, Shrinkage, and Durability of Concrete and Concrete Structures*, ASCE, Reston, VA.

Hlobil, M., Šmilauer, V., and Chanvillard, G. (2016). "Micromechanical multiscale fracture model for compressive strength of blended cement pastes." *Cem. Concr. Res.*, 83, 188–202.

Korte, S., and Clegg, W. (2009). "Micropillar compression of ceramics at elevated temperatures." *Scr. Mater.*, 60(9), 807–810.

Luczynski, K. W., Steiger-Thirsfeld, A., Bernardi, J., Eberhardsteiner, J., and Hellmich, C. (2015). "Extracellular bone matrix exhibits hardening elastoplasticity and more than double cortical strength: Evidence from homogeneous compression of non-tapered single micron-sized pillars welded to a rigid substrate." *J. Mech. Behav. Biomed. Mater.*, 52, 51–62.

Němeček, J., Králík, V., Šmilauer, V., Polívka, L., and Jäger, A. (2016). "Tensile strength of hydrated cement paste phases assessed by

Downloaded from ascelibrary.org by 18.234.201.198 on 11/08/21. Copyright ASCE. For personal use only; all rights reserved.

micro-bending tests and nanoindentation." *Cem. Concr. Compos.*, 73, 164–173.
Oliver, W. C., and Pharr, G. M. (2004). "Measurement of hardness and elastic modulus by instrumented indentation: Advances in understanding and refinements to methodology." *J. Mater. Res.*, 19(1), 3–20.
Pellenq, R. J., et al. (2009). "A realistic molecular model of cement hydrates." *Proc. Natl. Acad. Sci. U.S.A.*, 106(38), 16102–16107.
Pichler, B., et al. (2013a). "Effect of gel-space ratio and microstructure on strength of hydrating cementitious materials: An engineering micromechanics approach." *Cem. Concr. Res.*, 45, 55–68.
Pichler, B., et al. (2013b). "The counteracting effects of capillary porosity and of unhydrated clinker grains on the macroscopic strength of hydrating cement paste—A multiscale model." *Mechanics and Physics of Creep, Shrinkage, and Durability of Concrete: A Tribute to Zdeňk P. Bažant*, ASCE, Reston, VA, 40–47.
Pichler, B., and Hellmich, C. (2011). "Upscaling quasi-brittle strength of cement paste and mortar: A multi-scale engineering mechanics model." *Cem. Concr. Res.*, 41(5), 467–476.
Richardson, I., and Groves, G. (1993). "Microstructure and microanalysis of hardened ordinary portland cement pastes." *J. Mater. Sci.*, 28(1), 265–277.
Sarris, E., and Constantinides, G. (2013). "Finite element modeling of nanoindentation on C-S–H: Effect of pile-up and contact friction." *Cem. Concr. Compos.*, 36, 78–84.
Selvam, R. P., Subramani, V. J., Murray, S., and Hall, K. D. (2009). "Potential application of nanotechnology on cement based materials." National Academies of Sciences, Engineering, and Medicine, Washington, DC.
Shim, S., Bei, H., Miller, M. K., Pharr, G. M., and George, E. P. (2009). "Effects of focused ion beam milling on the compressive behavior of directionally solidified micropillars and the nanoindentation response of an electropolished surface." *Acta Materialia*, 57(2), 503–510.
Sneddon, I. N. (1965). "The relation between load and penetration in the axisymmetric Boussinesq problem for a punch of arbitrary profile." *Int. J. Eng. Sci.*, 3(1), 47–57.
Taylor, H. F. (1997). *Cement chemistry*, Thomas Telford, Langholm, U.K.
Tennis, P. D., and Jennings, H. M. (2000). "A model for two types of calcium silicate hydrate in the microstructure of portland cement pastes." *Cem. Concr. Res.*, 30(6), 855–863.
Uchic, M. D., and Dimiduk, D. M. (2005). "A methodology to investigate size scale effects in crystalline plasticity using uniaxial compression testing." *Mater. Sci. Eng. A*, 400, 268–278.
Uchic, M. D., Dimiduk, D. M., Florando, J. N., and Nix, W. D. (2003). "Exploring specimen size effects in plastic deformation of Ni ~ 3 (Al, Ta)." *Proc., Materials Research Society Symp.*, Materials Research Society, Warrendale, PA, 27–32.
Uchic, M. D., Dimiduk, D. M., Florando, J. N., and Nix, W. D. (2004). "Sample dimensions influence strength and crystal plasticity." *Science*, 305(5686), 986–989.
Vandamme, M., and Ulm, F. J. (2009). "Nanogranular origin of concrete creep." *Proc. Natl. Acad. Sci. U.S.A.*, 106(26), 10552–10557.
Volkert, C. A., and Lilleodden, E. T. (2006). "Size effects in the deformation of sub-micron Au columns." *Philos. Mag.*, 86(33–35), 5567–5579.
Yang, Y., Ye, J., Lu, J., Liu, F., and Liaw, P. (2009). "Effects of specimen geometry and base material on the mechanical behavior of focused-ion-beam-fabricated metallic-glass micropillars." *Acta Materialia*, 57(5), 1613–1623.
Ye, J., Lu, J., Yang, Y., and Liaw, P. (2010). "Extraction of bulk metallic-glass yield strengths using tapered micropillars in micro-compression experiments." *Intermetallics*, 18(3), 385–393.
Yilmaz, E. D., Bechtle, S., Özcoban, H., Schreyer, A., and Schneider, G. A. (2013). "Fracture behavior of hydroxyapatite nanofibers in dental enamel under micropillar compression." *Scr. Mater.*, 68(6), 404–407.
Yilmaz, E. D., Jelitto, H., and Schneider, G. A. (2015). "Uniaxial compressive behavior of micro-pillars of dental enamel characterized in multiple directions." *Acta Biomaterialia*, 16, 187–195.
Zhang, H., Schuster, B. E., Wei, Q., and Ramesh, K. T. (2006). "The design of accurate micro-compression experiments." *Scr. Mater.*, 54(2), 181–186.
Zhang, X., Zhao, Q., Wang, S., Trejo, R., Lara-Curzio, E., and Du, G. (2010). "Characterizing strength and fracture of wood cell wall through uniaxial micro-compression test." *Compos. Part A: Appl. Sci. Manuf.*, 41(5), 632–638.

Downloaded from ascelibrary.org by 18.234.201.198 on 11/08/21. Copyright ASCE. For personal use only; all rights reserved.